An algorithm for determination of the fracture angle for the three dimensional Puck matrix failure criterion for UD composites

J. Wiegand, N. Petrinic, B. Elliott

Accepted Manuscript

An algorithm for determination of the fracture angle for the three dimensional Puck matrix failure criterion for UD composites

J. Wiegand, N. Petrinic, B. Elliott

PII: S0266-3538(08)00185-1
DOI: 10.1016/j.compscitech.2008.05.004
Reference: CSTE 4075

To appear in: *Composites Science and Technology*

Received Date: 7 September 2007
Revised Date: 29 April 2008
Accepted Date: 2 May 2008

Please cite this article as: Wiegand, J., Petrinic, N., Elliott, B., An algorithm for determination of the fracture angle for the three dimensional Puck matrix failure criterion for UD composites, *Composites Science and Technology* (2008), doi: 10.1016/j.compscitech.2008.05.004

An algorithm for determination of the fracture angle for the three dimensional Puck matrix failure criterion for UD composites

J. Wiegand*, N. Petrinic, B Elliott

Department of Engineering Science, University of Oxford,

Parks Road, Oxford, OX1 3PJ

*Corresponding author. Tel +44 1865 273800; Fax +44 1865 273906; e-mail jens.wiegand@eng.ox.ac.uk

Keywords: Matrix cracking (B), Modelling (C), Failure criterion (C), Finite element analysis (FEA) (C), UD composites

Abstract:

A 3D matrix failure algorithm based upon Puck's failure theory has been developed. The problem of calculating the orientation of a potential fracture plane, which is necessary to assess the onset of matrix failure, has been addressed. Consequently, a fracture angle search algorithm is proposed. The developed algorithm incorporates a numerical search of function extremes which minimises the required computational time for finding the accurate orientation of a potential fracture plane. For illustration, the algorithm together with the three dimensional Puck failure model has been implemented in LS-DYNA explicit FE code. The fracture angle search algorithm is verified using a virtual uniaxial compression test.

1. INTRODUCTION

The development of physically based failure criteria for Inter Fibre Failure (IFF) in long fibre reinforced polymer composites has been the focus of research for many years. The first promising approach was proposed by Hashin [1] in 1980 who developed failure criteria for plane stress based on the Mohr Coulomb failure theory. The criteria stated that failure was caused by the stresses acting on an inclined fracture plane. However, Hashin did not pursue the calculation of the orientation of that plane because of the required computational effort. Further sound physical basis of the failure theory was posed by Puck [2] who extended the model, which now distinguishes three IFF modes: a) a tensile and b) a compressive shear matrix failure, in both of which the crack is perpendicular to direction 2-2, as well as c) a more complex failure mode in which the fracture plane rotates about 1-1 axis to form a wedge which can cause fibre failure in adjacent layers. Further suggestions for an extension to a 3D state of stress were made in [2]. An extensive experimental study in [3] verified the failure criteria for cases with plane stress states and three dimensional states of stress.

Initially, Puck's model was not well recognised in the research community. The reason was the large number of unknown parameters and the computationally expensive search of the fracture plane orientation. In order to simplify the application of the failure model, Puck proposed pragmatic solutions for some of the parameters in [4]. As the theory was ranked very highly in the World Wide Failure Exercise (WWFE) [5, 6] the model attracted additional attention and further development was undertaken by Davila and Camanho [7], Pinho et al [8] and Greve and Pickett [9].

The computationally expensive search for the angle of the fracture plane still remains a limiting factor. The application of the model in explicit Finite Element Analysis (FEA) requires a reliable, accurate, yet numerically efficient fracture plane orientation search algorithm. For plane stress, analytical formulations are already available [4]. The fracture angle for three dimensional states of stress, however, cannot be expressed in a closed form. Therefore, a numerical search procedure needs to be employed. So far, no efficient algorithms for finding the fracture plane angle for three dimensional states of stress have been proposed in open literature.

This paper introduces a computationally efficient fracture angle search algorithm of a full 3D Puck failure theory for IFF. The algorithm has been verified using a virtual uniaxial compression test and the capabilities of the overall model have been presented.

2. THE PUCK FAILURE CRITERION FOR IFF

The Puck IFF criteria are valid for UD composite laminates. The UD ply is treated as transverse isotropic and is assumed to behave in a brittle manner. The key idea of the Puck failure model is the assumption of a Mohr-Coulomb type of failure for loading transverse to the fibre direction. Failure is assumed to be caused by the normal and shear stresses which are acting on the stress action plane (σ_n, τ_{n1} and τ_{nt}, see Figure 1). Positive normal stress on this plane promotes fracture while negative normal stress increases the material's shear strength thus impeding fracture. Pucks stress based failure criteria enable the calculation of the material exposure e as a failure indicator. Failure occurs under the following condition

$$e = 1. \tag{1}$$

The values of e range between 0 (which denotes that material is not loaded) to 1 (which denotes the onset of IFF). A material exposure above 1 is physically inadmissible and denotes the initiation of damage of the material. The material exposure e is a function of the stress state $\boldsymbol{\sigma}$ and the orientation of the stress action plane against the thickness direction θ

$$e(\theta,\boldsymbol{\sigma})\,. \tag{2}$$

Fracture will occur on the stress action plane where $e(\theta,\boldsymbol{\sigma})$ has it's global maximum. This plane is called the fracture plane. The angle of the fracture plane is called the fracture angle θ_{fr}. The definition of fracture plane and fracture angle θ_{fr} is illustrated in Figure 1.

Puck's criteria define a master failure surface on the fracture plane. Only the stresses which act on that plane (Mohr's fracture plane stresses σ_n, τ_{n1} and τ_{nt}) are assumed to contribute to IFF. The fracture plane stresses are obtained by rotating the three dimensional stress tensor from material coordinates to the fracture plane. The relationship between the stresses in the ply coordinate system and the Mohr stresses in the inclined fracture plane reads

$$\begin{pmatrix}\sigma_1\\ \sigma_n\\ \sigma_t\\ \tau_{n1}\\ \tau_{nt}\\ \tau_{1t}\end{pmatrix}=\begin{pmatrix}1 & 0 & 0 & 0 & 0 & 0\\ 0 & c^2 & s^2 & 2cs & 0 & 0\\ 0 & s^2 & c^2 & -2cs & 0 & 0\\ 0 & 0 & 0 & c & 0 & s\\ 0 & -sc & sc & 0 & c^2-s^2 & 0\\ 0 & 0 & 0 & -s & 0 & c\end{pmatrix}\begin{pmatrix}\sigma_{11}\\ \sigma_{22}\\ \sigma_{33}\\ \sigma_{12}\\ \sigma_{23}\\ \sigma_{13}\end{pmatrix} \tag{3}$$

with

$$
\begin{aligned}
c &= \cos(\theta_{fr}) \\
s &= \sin(\theta_{fr})
\end{aligned}
\tag{4}
$$

From Figure 1 it can be seen that only σ_n, τ_{n1} and τ_{nt} contribute to IFF. The fracture plane tractions are given by

$$
\begin{aligned}
\sigma_n &= \sigma_{22}\cos^2\theta_{fr} + \sigma_{33}\sin^2\theta_{fr} + 2\sigma_{23}\cos\theta_{fr}\sin\theta_{fr}, \\
\tau_{n1} &= \sigma_{12}\cos\theta_{fr} + \sigma_{13}\sin\theta_{fr} \\
\tau_{nt} &= -\sigma_{22}\sin\theta_{fr}\cos\theta_{fr} + \sigma_{33}\sin\theta_{fr}\cos\theta_{fr} + \sigma_{23}(\cos^2\theta_{fr} - \sin^2\theta_{fr}).
\end{aligned}
\tag{5}
$$

From Eqns (5) it is clear that all components of stress tensor, except σ_{11}, contribute to IFF.

The master failure surface on the fracture plane is defined in terms of Mohr-Coulomb fracture plane stresses thus yielding the following failure criteria

$$
\begin{aligned}
e &= \left(\frac{\sigma_n}{R_n}\right)^2 + \left(\frac{\tau_{n1}}{R_{n1} - p_{n1}\sigma_n}\right)^2 + \left(\frac{\tau_{nt}}{R_{nt} - p_{nt}\sigma_n}\right)^2 = 1 \quad \text{for } \sigma_\mathrm{n} \geq 0 \\
e &= \left(\frac{\tau_{n1}}{R_{n1} - p_{n1}\sigma_n}\right)^2 + \left(\frac{\tau_{nt}}{R_{nt} - p_{nt}\sigma_n}\right)^2 = 1 \quad \text{for } \sigma_\mathrm{n} < 0.
\end{aligned}
\tag{6}
$$

In order to evaluate Eqn (6) it is essential that θ_{fr} is known. The parameters in Eqn (6) are defined as follows (see [4]):

- R_n: resistance of the fracture plane against normal failure
- R_{n1}, R_{nt}: resistance of the fracture plane against shear
- p_{n1}, p_{nt}: slope parameters representing internal friction effects (Mohr-Coulomb type of failure).

Unlike traditional failure criteria, Puck uses fracture plane resistances R. The fracture plane resistance is the resistance of the material against fracture caused by only one component of stress acting on that plane [4]. Two of these values can be obtained directly from simple uniaxial or shear experiments and are identical to the respective strength properties

$$
\begin{aligned}
R_n &= Y_t\,, \\
R_{n1} &= S_{12}\,.
\end{aligned}
\tag{7}
$$

The fracture plane resistance R_{nt} usually cannot be measured directly. The reason is, that unidirectional fibre reinforced composite materials (e.g. GFRP CFRP) when subjected to a pure transverse shear loading (σ_{23}) fail at an angle $\theta_{fr} \approx 45^\circ$. In order to assume $R_{nt} = S_{23}$ the failure must happen in the same plane where σ_{23} is acting as a single stress (eg. $\theta_{fr} = 0^\circ$ or $\theta_{fr} = 90^\circ$). In fact, what could be measured as shear strength S_{23}, denotes not a pure shear failure, but a failure due to single normal tensile stress acting on the fracture plane [2] (see stress state1 in Table 2). Puck proposes to calculate R_{nt} from uniaxial compression tests. Specimens loaded uniaxially transverse to the fibre tend to fail by a shear failure on a fracture plane which is inclined by θ_{fr}^0. This and the experimentally observed compressive stress at failure Y_c allow calculating the stress state at failure on the fracture plane. Further assumption of a Mohr Coulomb type failure allows for the shear stress at failure τ_{nt} to be obtained in the case of $\sigma_n = 0$. This is the missing fracture plane resistance R_{nt} (see Eqn. (8)).

The slope parameters p_{n1} and p_{nt} characterise the slope of the fracture envelope at $\sigma_n = 0$ and can be derived experimentally by combined loading experiments [4].

The experimental data necessary to define fully the failure surface is usually not available. Puck gives some pragmatic solutions for the parameters to be derived from simple uniaxial compression experiments [4]. The "missing" parameters are evaluated as follows:

$$
\begin{aligned}
R_{nt} &= \frac{Y_c}{2\tan\theta_{fr}^0}, \\
p_{nt} &= -\frac{1}{2\tan(2\theta_{fr}^0)}, \\
p_{n1} &= p_{nt}\frac{R_{n1}}{R_{nt}}.
\end{aligned}
\tag{8}
$$

This fully defines the master failure surface. An example of a master failure surface obtained using the data in Table 1 is plotted in Figure 2. The failure surface is open for negative σ_n because compressive stress σ_n impedes IFF.

The master failure surface is not normally used directly in the design of components made of UD composite materials since stress analysis usually relies upon the assessment of stress state in the material coordinate system. For known fracture angles the master failure surface can be projected on the material coordinate system. Two projected failure surfaces in σ_{22}-σ_{33}-σ_{12} stress space and σ_{22}-σ_{33}-σ_{23} stress space are plotted as examples in Figure 3. Please note that due to symmetry in respect to the σ_{22}-σ_{33} plane, only half of the failure surfaces are plotted in Figure 3

Cutting a section of the projected failure surfaces in Figure 3 allows plotting of the commonly used failure envelopes $\sigma_{22}-\sigma_{12}$ (plane $\sigma_{23}=0$) and $\sigma_{22}-\sigma_{23}$ (plane $\sigma_{12}=0$) which are displayed in Figure 4. The failure surfaces and envelopes have been obtained using the constitutive parameters listed in Table 1.

3. DETERMINATION OF THE FRACTURE ANGLE

It is clear from Eqn (5) and (6) that the material exposure e for IFF is a function of all components of stress (except σ_{11}) and the fracture angle

$$e(\sigma_{22},\sigma_{33},\sigma_{12},\sigma_{23},\sigma_{13},\theta_{fr})\,. \tag{9}$$

Hence, failure can only be assessed if the fracture angle is known. Ability to calculate θ_{fr} requires further understanding of the relationship between the material exposure e and the orientation of the action plane θ. The material exposure e can be presented graphically for a fixed stress states while allowing for θ to vary. Due to symmetry the range of θ can be limited to $-90^\circ \le \theta \le 90^\circ$ [2]. In Figure 5 $e(\theta)$ is plotted for the stress states presented in Table 2. From Figure 5 it becomes clear that the fracture plane orientation is given by the angle for which the function $e(\theta)$ reaches the global maximum, which denotes the critical stress action plane. Hence, the fracture angle θ_{fr} is given by

$$e(\theta_{fr}) = \max e(\theta). \tag{10}$$

Stress state 1 in Figure 5 would therefore cause fracture in a plane inclined by $\theta_{fr} = 45^\circ$ as observed experimentally. According to [2] $e(\theta)$ only has one global maximum in the interval $-90^\circ \le \theta \le 90^\circ$. However, it can be shown that for special cases the function $e(\theta)$ has two global extremes (as illustrated in Figure 5 for stress state 3). The function $e(\theta)$ is then symmetric and two theoretical fracture angles (same magnitude, but alternating sign) are possible.

The calculation of the fracture angle therefore turns into a search for the global maximum of the function $e(\theta)$ within the interval $-90^\circ \le \theta \le 90^\circ$. For 2D stress states analytical solutions exist, however, for three dimensional stress states analytical solutions have not been proposed yet.

The lack of analytical solutions requires numerical solutions to be applied. The fracture angle θ_{fr} can be obtained by calculating $e(\theta)$ at a certain number of angles θ in the domain $-90^\circ \le \theta \le 90^\circ$. The accuracy of θ_{fr} then depends upon the number of angles θ for which $e(\theta)$ has been evaluated. This stepwise scan of $e(\theta)$ is a computationally very expensive procedure since for every point of $e(\theta)$ the stress tensor has to be rotated by θ.

An efficient and accurate numerical algorithm for evaluation of the global maximum of $e(\theta)$ is proposed in this paper. Numerical bisection methods for bracketing the extremes of one dimensional functions have been studied and the Golden Section Search [10] has been adapted to the problem of finding the fracture plane angle. In the remainder of this section the developed numerical algorithms are introduced which enable a robust approach to determination of the fracture angle.

3.1. Golden Section Search

The Golden Section Search is a function maximisation/minimisation technique. The technique only applies to functions where an extreme is known to exist within the search range. The extreme is found by successively narrowing the search range by evaluating the function at triples of points. The distances of these points form Golden Ratios which gives the technique its name.

The function $e(\theta)$ is evaluated at θ_1, θ_2 and θ_3. The angle θ_3 is chosen by means of

$$\frac{b}{a} = \varphi \tag{11}$$

with φ being the golden ratio

$$\varphi = \frac{1+\sqrt{5}}{2}. \tag{12}$$

An additional point $e(\theta_4)$ is evaluated. The position of the point is chosen as follows

$$\frac{b}{a} = \frac{a}{c} \tag{13}$$

thus guaranteeing that θ_4 is symmetric to θ_3 in the original search range. The decision how to narrow the search range in the next calculation step is taken by comparing $e(\theta_3)$ and $e(\theta_4)$. In case $e(\theta_4) \geq e(\theta_3)$ (indicated as $e(\theta_{4\mathrm{b}})$ in Figure 6) the new search range is limited by θ_3 and θ_2, otherwise (indicated as $e(\theta_{4\mathrm{a}})$ in Figure 6) the search continues between θ_1 and θ_4. The choice of φ as ratio guarantees that the extreme is bracketed in the larger section which leads to an optimal method of function maximisation [10]. The iterative maximum search is performed until the distance between the outer points of the bracket is tolerably small. The decision what is tolerably small should be linked to the expected accuracy for θ_{fr}. Since the accurate value for θ_{fr} is definitely somewhere between the outer bounds $e(\theta_1)$ and $e(\theta_2)$, the distance

$$k = \theta_2 - \theta_1 \tag{14}$$

is compared with the exit criterion k_{exit}. The iteration is stopped when the condition

$$k = k_{\mathrm{exit}} \tag{15}$$

is satisfied. Thereby k_{exit} denotes the lowest guaranteed accuracy of the obtained fracture angle θ_{fr}. An example for the Golden Section search is illustrated in Figure 7.

3.2. *Extended Golden Section Search*

Figure 7 shows that the Golden Section Search algorithm quickly brackets the maximum, but needs a quite large number of iterations to find the accurate value for θ_{fr}. It is therefore proposed to combine the Golden Section Search with a curve interpolation technique called Inverse Parabolic Interpolation [10].

Initially, the Golden Section search is used to bracket the maximum sufficiently accurately. It is then assumed that $e(\theta)$ can be approximated by a parabola near the already bracketed maximum. The upper and lower bound of the last Golden Section Search iteration and an arbitrary point between them are chosen to define a parabola. These three points $P_1(\theta_1, e(\theta_1))$, $P_2(\theta_2, e(\theta_2))$ and $P_3(\theta_3, e(\theta_3))$ fully define the parabola $p(\theta)$ by

$$
\begin{aligned}
p(\theta) = e(\theta_1)\frac{(\theta-\theta_2)(\theta-\theta_3)}{(\theta_1-\theta_2)(\theta_1-\theta_3)} + e(\theta_2)\frac{(\theta-\theta_1)(\theta-\theta_3)}{(\theta_2-\theta_1)(\theta_2-\theta_3)} + \\
e(\theta_3)\frac{(\theta-\theta_1)(\theta-\theta_2)}{(\theta_3-\theta_1)(\theta_3-\theta_2)}
\end{aligned}
\tag{16}
$$

As the maximum of $p(\theta)$ is normally sufficiently close to the sought maximum of $e(\theta)$ the following approximation for θ_{fr} is adopted

$$
\theta_{fr} \approx \theta_2 - \frac{1}{2}\frac{(\theta_2-\theta_1)^2(e(\theta_2)-e(\theta_3)) - (\theta_2-\theta_3)^2(e(\theta_2)-e(\theta_1))}{(\theta_2-\theta_1)(e(\theta_2)-e(\theta_3)) - (\theta_2-\theta_3)(e(\theta_2)-e(\theta_1))}. \tag{17}
$$

Thus, the unnecessary iterations close to the maximum of $e(\theta)$ are avoided without compromising the accuracy of the algorithm. An example for the extended Golden Section Search is illustrated in Figure 8.

3.3. *Numerical efficiency*

The application of the Puck IFF model in an explicit FE environment requires a fast fracture angle search algorithm to find the fracture plane. Within the fracture angle search, the transformation of the stress state from material coordinates on the fracture plane is the most computationally expensive step. The algorithm which evaluates the smallest number of values of $e(\theta)$ for a given accuracy, will give the most numerically efficient solution. Following, the three approaches, stepwise scan of $e(\theta)$, Golden Section Search and extended Golden Section Search are judged for their numerical efficiency. The assessment of the numerical efficiency presented is performed using stress state 1 in Table 2. The required number of values of $e(\theta)$ depends on the respective stress state, but similar results have been achieved for other stress states. The stepwise scan is performed using a decreasing scanning step allowing for an assessment of scan step and fracture angle accuracy. The Golden Section search and the extended Golden Section search were performed for decreasing values of the exit criterion which results in a increasing number of evaluated points and a decreasing error for θ_{fr}. The quoted error was calculated using the fracture angle θ_{fr} obtained from a stepwise scan with a scanning step of 0.01°. The comparison of the results is presented in Figure 9.

Figure 9 demonstrates the advantages of the extended Golden Section Search. Reliable fracture angles are already calculated from as few as 6 evaluated points. The Golden Section search already needs 13 points for a similar accuracy. The stepwise scan fails to predict the fracture angle with similar accuracy for a scanning step greater then one, which results in 180 and more necessary evaluated points. It should be noted that the extended Golden Section Search requires at least 4 evaluated points and the Golden Section Search requires at least 2 data points. For this reason no error is quoted below these values.

4. VERIFICATION OF THE FRACTURE ANGLE SEARCH

The reliability of the fracture angle algorithm is demonstrated by a comparison of reference fracture envelopes obtained by dense stepwise scanning $e(\theta)$ and envelopes obtained using the proposed fast angle search algorithm. The reference values of function $e(\theta)$ were calculated by varying the angle by 0.5° for every successive data point thus giving a reliable prediction of the fracture angle for comparison. The failure envelopes predicted using the extended Golden Section Search algorithm are displayed in Figure 10.

It is demonstrated that the proposed fracture angle search algorithm reliably finds the correct fracture angles. The fracture angle prediction obtained using the extended Golden Section Search algorithm is virtually identical to that obtained by the computationally expensive stepwise scan of $e(\theta)$ thus resulting in practically identical failure envelopes.

The proposed fracture angle algorithm is suitable for application in both implicit and explicit FE. The implementation of the new fracture angle search algorithm in explicit FE, in particular, has already promoted the use of the 3D Puck failure model in aerospace and marine applications of authors' interest. To-date, due to the computational cost of the fracture angle search, the application of this sophisticated failure theory was prohibitive. For illustration, the algorithm has been implemented in the commercially available explicit FE solver LS-DYNA which enabled a virtual uniaxial compression test to be used for verification of the proposed algorithm. The aim of the simulation was to demonstrate that the potential fracture plane can be predicted by the model and that the fracture angle search works reliably for 3D states of stress. For the calculation of the material exposure, the constitutive parameters given in Table 1 were used. Since no experimental results were available within this study, experimental results presented in [3] are given for comparison. The FE model and its results along side with the experimental results [3] are presented in Figure 11.

The material exposure is accurately predicted to be the highest at the same locations within the specimen's gauge section where the experiments showed the evidence of IFF. The contour plot of the material exposure in Figure 11 shows that the highest values form a plane whose slope is inclined by θ_{fr}^{0} from the loading direction. A potential failure initiates near an edge due to stress concentrations as expected. Due to symmetry the FE model predicts two crossing planes of a potential failure. In experiments only one fracture plane is observed, usually triggered by imperfections. The example shows that the newly implemented fracture angle search, as a part of the Puck failure model, is able to predict correctly the potential fracture plane thus promising realistic predictions of matrix failure in the design of composite components.

5. CONCLUSIONS

A variant of Puck failure model for predictive modelling of matrix failure in 3D has been implemented into LS-DYNA for explicit FE simulations. In this paper, the problem of fracture angle calculation is outlined and potential solutions are presented. On that basis, an accurate and numerically efficient fracture angle search algorithm was developed. The proposed algorithm is expected to become widely used given the recent increased interest in three dimensional failure theory. Further potential applications might arise with the outcome of the World Wide Failure Exercise II (WWFEII), which is currently ongoing.

Failure envelopes, calculated using the proposed fracture angle search algorithm, are compared with an accurate but computationally expensive method of predicting the fracture plane angle in Puck's model. The comparison demonstrates the accuracy of the newly proposed approach. Additionally, a virtual uniaxial compression test was performed. The predicted fracture plane was in good agreement with results of similar experiments.

The FE implementation of the fracture angle search algorithm enables a wider application of the Puck failure model for the design of composite components and structures. Puck's physically based failure theory has been proven to be more realistic compared to other theories [6]. The future work will focus onto generating a more elaborate experimental data set based on simple and complex 3D stress states for validation of the fracture angle search algorithm and the constitutive model as a whole. The implementation of the Puck IFF failure model as presented here will be part of a three dimensional composite damage model, which is currently under development.

Acknowledgments

This research has been sponsored by the EU (VITAL, FP6-012271) and Rolls-Royce plc whose support is kindly acknowledged.

6. REFERENCES

1. Hashin Z. Failure Criteria for Unidirectional Fibre Composites. Journal of Applied Mechanics 1980; 47: 329-334.

2. Puck A. Festigkeitsanalyse von Faserverbundlaminaten. Muenchen: Carl Hanser Verlag, 1996.

3. Cuntze RG, Deska R, Szelinski B, JeltschFricker R, Meckbach S, Huybrechts D, Kopp J, Kroll L, Gollwitzer S, Rackwitz R. Neue Bruchkriterien und Festigkeitsnachweise fuer unidirektionalen Faserkunststoffverbund unter mehrachsiger Beanspruchung -Modellbildung und Experimente. In: VDI Fortschritt-Berichte. Duesseldorf: VDI Verlag, 1997.

4. Puck A, Kopp J, Knops M. Guidelines for the determination of the parameters in Puck's action plane strength criterion. Composites Science and Technology 2002; 62(3): 371-378.

5. Hinton MJ, Soden PD. Predicting failure in composite laminates: The background to the exercise. Composites Science and Technology 1998; 58(7): 1001-1010.

6. Kaddour AS, Hinton MJ, Soden PD. A comparison of the predictive capabilities of current failure theories for composite laminates: additional contributions. Composites Science and Technology 2004; 64: 449-476.

7. Davila GC, Camanho PP. Failure Criteria for FRP Laminates in plane Stress. Tech. Rep. 2003; NASA/TM-2003-212663.

8. Pinho ST, Iannucci L, Robinson P. Physically-based failure models and criteria for laminated fibre-reinforced composites with emphasis on fibre kinking: Part I: Development. Composites Part a-Applied Science and Manufacturing 2006; 37(1): 63-73.

9. Greve L, Pickett AK. Modelling damage and failure in carbon/epoxy non-crimp fabric composites including effects of fabric pre-shear. Composites Part a-Applied Science and Manufacturing 2006; 37(11): 1983-2001.

10. Press WH, Teukolsky SA, Vetterling WT, Flannery BP. Numerical Recipes in C. New York: Cambridge University Press, 1992.

Figures and captions

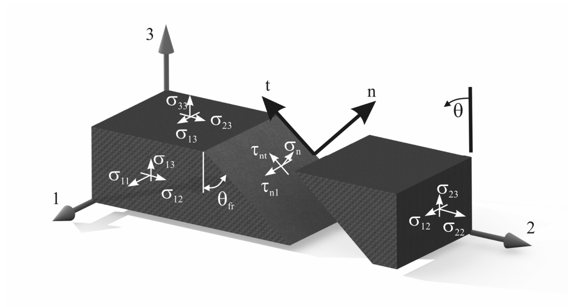

Figure 1 Definition of the fracture plane by the fracture angle θ_{fr} for the Puck IFF model

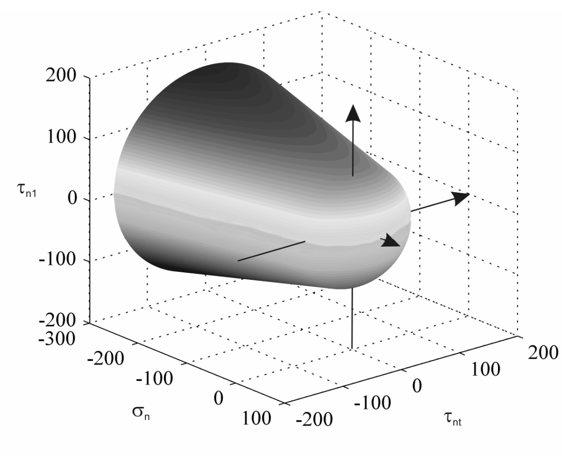

Figure 2 The master failure surface described by Eqn (6) computed using the parameters in Table 1

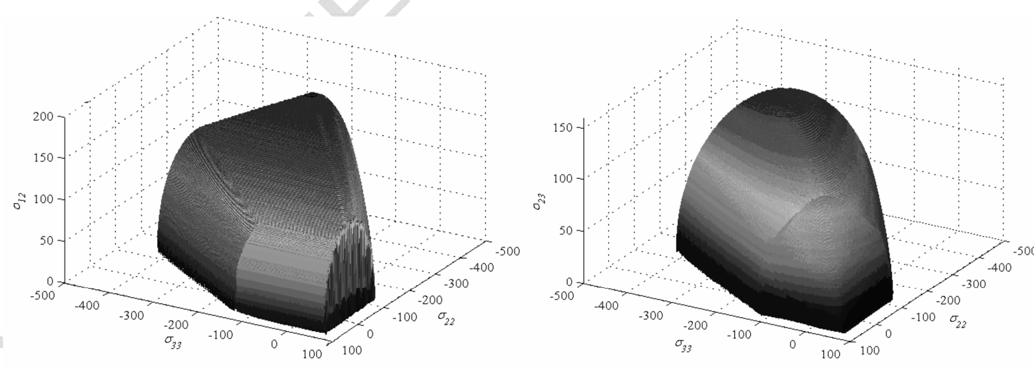

a) master failure surface projected in σ_{22} σ_{33} σ_{12} space   b) master failure surface projected in σ_{22} σ_{33} σ_{23} space

Figure 3 Projection of the master failure surface on the material coordinate system

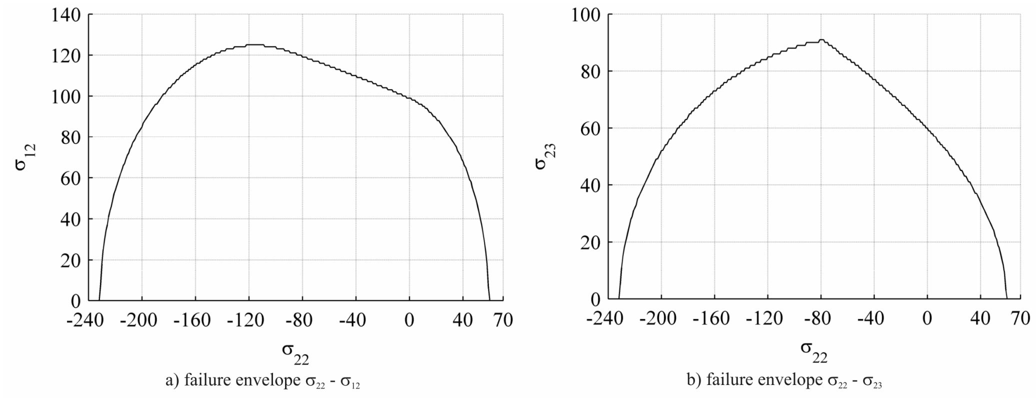

Figure 4 Example of the projection of the master failure surface on the material coordinates

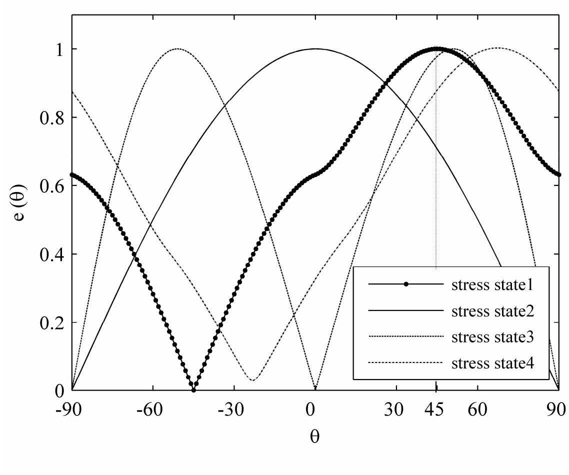

Figure 5 The stress action plane dependent material exposure for the stress states in Table 2

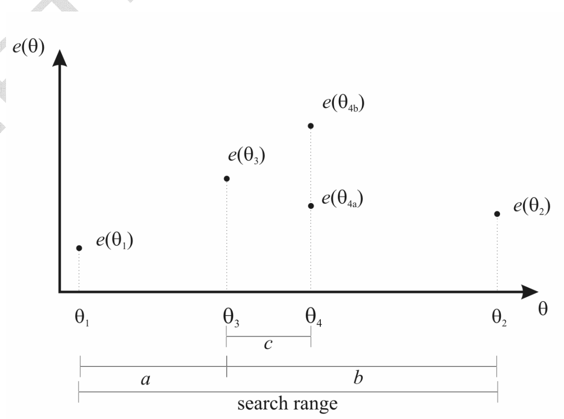

Figure 6 Golden Section Search algorithm schematic

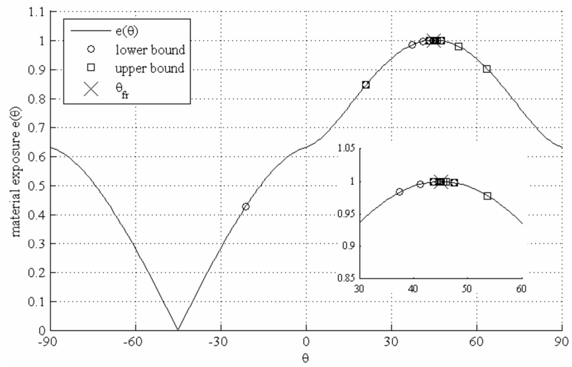

Figure 7 Fracture angle search by Golden Section Search

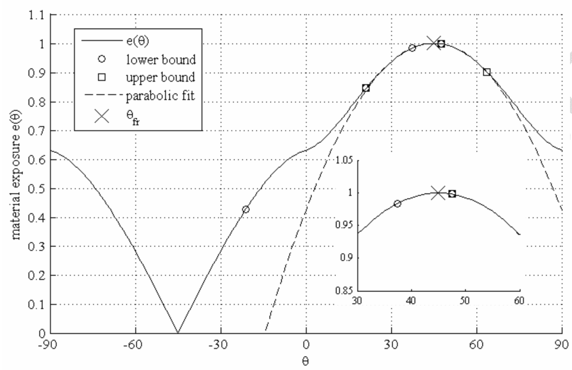

Figure 8 Fracture angle search by extended Golden Section Search

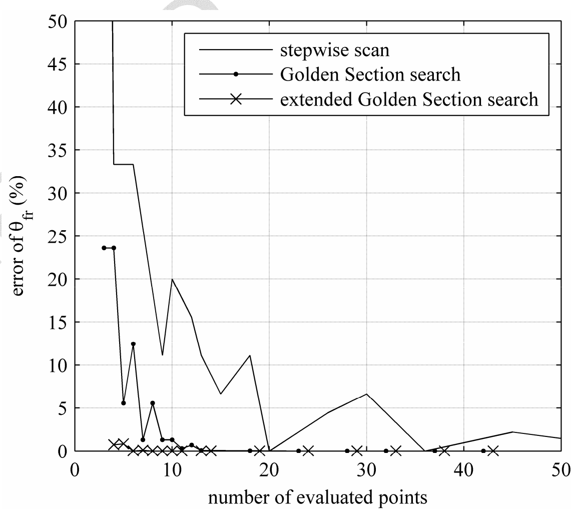

Figure 9 Assessment of numerical efficiency and accuracy of the fracture angle search algorithms

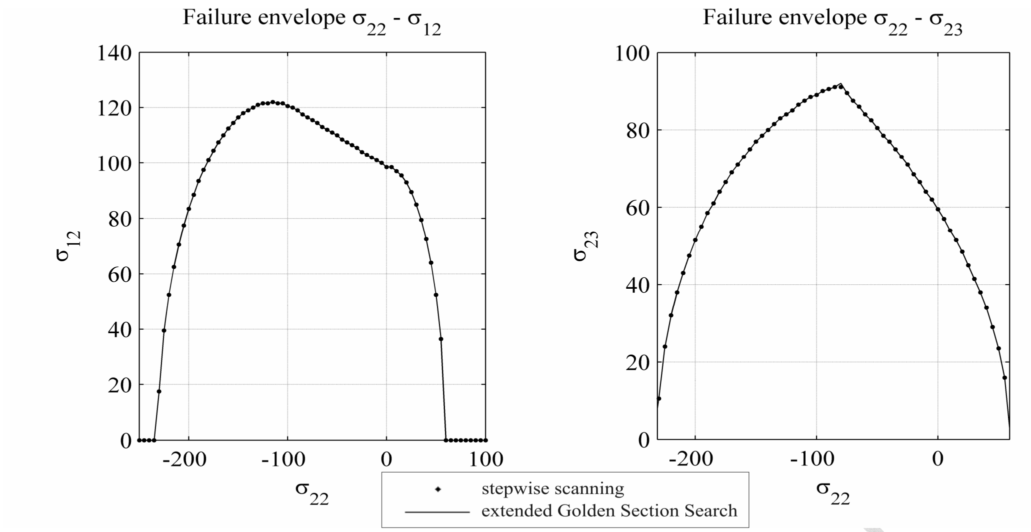

Figure 10 Verification of the fracture angle algorithm by comparison of failure envelope obtained by stepwise scanning of e(θ) and the extended Golden Section Search

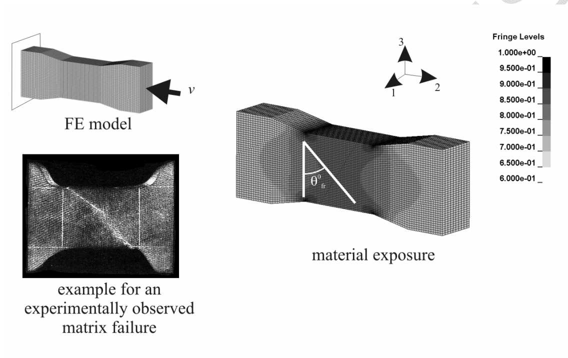

Figure 11 Application example: uniaxial compression of UD composite transverse to the fibres (image of the failed specimen reproduced from [3])

Tables

Table 1 Typical properties for a Carbon Epoxy composite [3]

tensile strength 2 direction	Y_t	59.1 MPa
compressive strength 2 direction	Y_c	231.2 MPa
in plane shear strength	S_{12}	98.4 MPa
fracture angle for pure compression	θ_{fr}^0	51°

Table 2 Example stress states for which the Puck failure model predicts IFF (calculated using properties in Table 1)

stress state	σ_{11}	σ_{22}	σ_{33}	σ_{12}	σ_{23}	σ_{13}	σ_n	τ_{n1}	τ_{nt}	θ_{fr}
1 (pure shear)	0.0	0.0	0.0	0.0	59.1	0.0	59.1	0.0	0.0	45°
2 (pure shear)	0.0	0.0	0.0	98.4	0.0	0.0	0.0	98.4	0.0	0°
3 (uniaxial compression)	0.0	-231.2	0.0	0.0	0.0	0.0	-92.0	0.0	-113.2	51°
4 (arbritary 3D)	0.0	-10.0	40.0	21.0	24.0	43.3	49.7	47.8	0.75	67°